

# Integrated Long-range Sensing and Communications in Multi Target Scenarios using CP-OFDM

Benedikt Geiger\*, Silvio Mandelli<sup>†</sup>, Marcus Henninger<sup>†</sup>, Daniel Gil Gaviria\*, Charlotte Muth\*, Laurent Schmalen\*

\*Communications Engineering Lab (CEL), Karlsruhe Institute of Technology (KIT), 76187 Karlsruhe, Germany

<sup>†</sup>Nokia Bell Labs Stuttgart, 70469 Stuttgart, Germany

Email: benedikt.geiger@kit.edu

**Abstract**—6G communication systems promise to deliver sensing capabilities by utilizing the orthogonal frequency division multiplexing (OFDM) communication signal for sensing. However, the cyclic prefix inherent in OFDM systems limits the sensing range, necessitating compensation techniques to detect small, distant targets like drones. In this paper, we show that state-of-the-art coherent compensation methods fail in scenarios involving multiple targets, resulting in an increased noise floor in the radar image. Our contributions include a novel multi target coherent compensation algorithm and a generalized signal-to-interference-and-noise ratio for multiple targets to evaluate the performance. Our algorithm achieves the same detection performance at long distances requiring only 3.6% of the radio resources compared to classical OFDM radar processing. This enables resource efficient sensing at long distances in multi target scenarios with legacy communications-only networks.

## I. INTRODUCTION

By leveraging the communication signal also for sensing, integrated sensing and communications (ISAC) has the potential to transform the sixth generation (6G) of mobile communication networks, enabling the detection of passive objects in a radar-like manner [1]. ISAC promises reduced hardware complexity, higher spectral efficiency as well as energy efficiency compared to two separate systems, and novel use cases such as drone detection, which is a rapidly growing market [2], [3].

Like the current versions of cellular standards, 6G ISAC systems are expected to utilize orthogonal frequency division multiplexing (OFDM) because it allows for efficient equalization and channel estimation in the frequency domain (FD) using the fast Fourier transform (FFT). To satisfy the periodicity requirement of the FFT at the communication receiver, a cyclic prefix (CP), which is longer than the delay spread of the communication channel, is added to the transmit symbols. In theory, the delay spread is infinite, but in practice, the belated reflections tend to be very weak, and the delay spread of the communications channel is limited to the relevant, i.e., strong, taps. While weak reflections exceeding the duration of the CP do not significantly degrade communication, ISAC systems should be capable of detecting objects that exceed the CP duration. However, if the delay of an object exceeds the CP duration, part of the reflection spills into the consecutive

This work has received funding from the German Federal Ministry of Education and Research (BMBF) within the projects Open6GHub (grant agreement 16KISK010) and KOMSENS-6G (grant agreement 16KISK123 and grant agreement 16KISK112K).

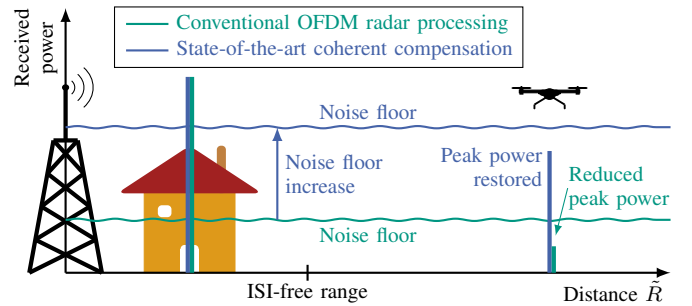


Fig. 1. Scenario under investigation: Long-range drone detection in a multi target scenario using a communication-centric CP-OFDM-ISAC system. The drone remains undetected using both algorithms. This highlights the need for a novel long-range sensing algorithm that works robustly in multi target scenarios. Conventional OFDM radar processing suffers from a reduced peak power. The state-of-the-art CC, which increases the signal power of distant targets, disproportionately increases the interference-and-noise floor, further preventing drone detection.

OFDM symbol leading to inter-symbol interference (ISI) and inter-carrier interference (ICI). As a result, the range corresponding to the CP duration is often referred to as ISI-free range [4], which, for example, is only 343m in case of a normal CP duration at 30 kHz sub-carrier spacing [5]. More critically, the portion of the reflection that overlaps with the consecutive OFDM symbol is not present in the actual OFDM symbol, reducing the target's peak power in the range-Doppler matrix (RDM), which could result in a missed detection, as visualized in the distant drone detection scenario in Fig. 1.

To address this limitation, time domain channel estimation can be used to detect targets beyond the ISI-free range [6]. However, this method significantly increases computational complexity compared to conventional FFT-based processing [6]. Alternatively, Wang et al. [7] proposed a coherent compensation (CC) algorithm that increases the peak power of the distant target by adding the current OFDM symbol to the previous one. While this method operates in the frequency domain with only a slight increase in complexity, it introduces significant ISI in multi target scenarios, which can be much stronger than the resulting signal power increase, as shown in Fig. 1, making it impractical for real-world applications. Thus, ISAC systems lack a low-complexity, long-range sensing algorithm that can robustly handle multi target scenarios.

In this paper, we address this gap by investigating sensing beyond the ISI-free range in multi target scenarios using a CP-OFDM-ISAC system. Our contributions include:

- We derive the image signal-to-interference-and-noise ratio (SINR) for scenarios where targets exceed the ISI-free range.
- We determine the maximum detection range of distant targets with a small radar cross section (RCS) using a communication-centric ISAC system demonstrating the need for a long-range sensing algorithm.
- We demonstrate the ISI issue of the state-of-the-art CC method in multi target scenarios.
- We propose a novel multi target coherent compensation (MTCC) algorithm for robust long-range sensing in multi target scenarios.
- We verify all our results through simulations.

## II. SYSTEM MODEL

In this paper, we consider a monostatic OFDM-ISAC system in which a sensing receiver is co-located with the transmitter, e.g., a base station. The co-location of the transmitter and sensing receiver ensures synchronization and allows the sensing receiver to access the transmitted data. The ISAC system follows a communication-centric design and transmits information to mobile users while simultaneously sensing the environment based on the reflections of the transmit signal. Figure 2 shows a block diagram of the signal processing architecture that we detail in the following.

### A. Transmitter

One OFDM frame consists of  $M$  OFDM symbols, each using  $N$  orthogonal sub-carriers with sub-carrier spacing  $\Delta f = B/N = 1/(T_s N) = 1/T$ , where  $B$ ,  $T_s$ , and  $T$  denote bandwidth, sample duration, and OFDM symbol duration, respectively. The transmitter modulates the constellation symbols  $X[n, m]$  ( $n = 1, \dots, N, m = 1, \dots, M$ ) from a modulation alphabet  $\mathcal{A}$ , e.g., QPSK, and adds a CP to each symbol before transmitting the equivalent baseband signal [8]

$$s(t) = \frac{1}{\sqrt{N}} \sum_{m=1}^M \sum_{n=1}^N X[n, m] e^{j2\pi n \Delta f (t - mT_0)} g(t - mT_0), \quad (1)$$

where  $T_0 = T + T_{cp}$  is the OFDM symbol duration incl. CP and  $g(t) = \text{rect}_{[-T_{cp}, T]}(t)$  is a rectangular function  $\text{rect}_{[a, b]}(t)$ , which is 1 if  $t \in [a, b]$  and 0 otherwise.

### B. Sensing Channel Model

Assuming a Swerling-0 model [9] and  $H$  point targets each having a distance  $R_h$ , radial velocity  $v_h$  and RCS  $\sigma_{\text{RCS}, h}$ , the received sensing signal is [8]

$$r(t) = \sum_{h=1}^H a_h s(t - \tau_h) e^{j2\pi(f_{D, h} t + \varphi_h)} + w(t), \quad (2)$$

where amplitude  $a_h$ , delay  $\tau_h$ , and Doppler frequency  $f_{D, h}$  of target  $h$  are [8]

$$a_h = \sqrt{\frac{\sigma_{\text{RCS}, h} c_0^2 P_{\text{Tx}} G_{\text{Tx}} G_{\text{Rx}}}{(4\pi)^3 R_h^4 f_c^2}}, \quad \tau_h = 2 \frac{R_h}{c_0}, \quad f_{D, h} = 2 \frac{v_h f_c}{c_0}. \quad (3)$$

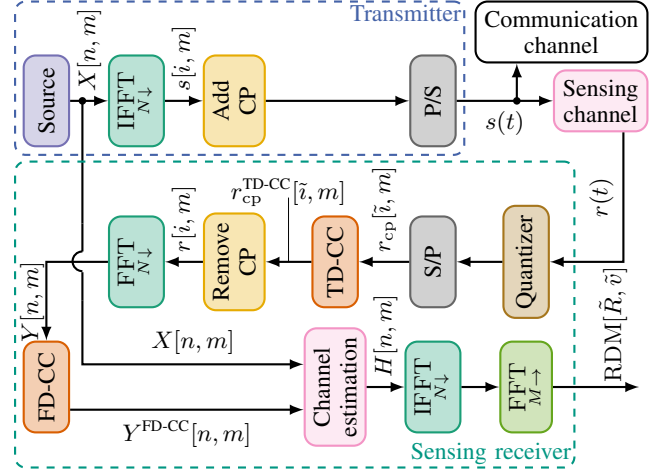


Fig. 2. Block diagram of the OFDM ISAC signal processing architecture including the TD- and FD-CC assuming an ideal radio frequency frontend.

The parameters  $P_{\text{Tx}}$ ,  $G_{\text{Tx}}$ ,  $G_{\text{Rx}}$ ,  $f_c$ , and  $c_0$  represent transmit power, gain of the transmit and receive antenna, carrier frequency and speed of light, respectively. The phase  $\varphi_h$  is uniformly sampled from the interval  $[0, 2\pi)$  and the thermal noise is  $w(t) \sim \mathcal{CN}(0, \sigma_{\text{Therm}}^2)$ , with noise power  $\sigma_{\text{Therm}}^2 = FkBT_{\text{Therm}}$ . Here,  $k$  is Boltzmann's constant,  $T_{\text{Therm}}$  the equivalent noise temperature, and  $F$  the noise figure of the receiver.

### C. Receiver

At the sensing receiver, the received signal  $r(t)$  is filtered, sampled, quantized using  $Q$  bits, and the CP is removed. Next, the signal is transformed into the frequency domain by taking the FFT along the  $N$  sub-carriers. In the frequency domain, the channel is estimated by an element-wise division of the receive symbols by the transmit symbols

$$H[n, m] = \frac{Y[n, m]}{X[n, m]} \odot H_{\text{win}}[n, m], \quad (4)$$

where  $\odot$  is the Hadamard product and  $H_{\text{win}}$  a windowing function to suppress sidelobes in the RDM. Finally, the RDM matrix is obtained by an orthonormal inverse fast Fourier transform (IFFT) along the sub-carriers, and an orthonormal FFT along the OFDM symbols [8]

$$\text{RDM}[\check{R}, \check{v}] = \text{FFT}_{M \rightarrow} \left\{ \text{IFFT}_{N \downarrow} \{H[n, m]\} \right\}. \quad (5)$$

### D. Distant Targets

Since the CP is optimized for communications and not for sensing, the delay of a target of interest (TOI) can easily exceed the duration of the CP. For a delay  $0 \leq \tau_h < T$ , the  $h$ th target's contribution to the  $m$ th received symbol after CP removal is [7]

$$r_h[i, m] = \frac{1}{\sqrt{N}} \left( \sum_{n=1}^N X[n, m] e^{j2\pi n \Delta f (iT_s - \tau_h)} g(iT_s - \tau_h) + \sum_{n=1}^N X[n, m-1] e^{j2\pi n \Delta f (iT_s - \tau_h + T_0)} g(iT_s - \tau_h + T_0) \right) \tilde{a}_h[m], \quad (6)$$

where  $i = 1, \dots, N$  denotes the sample in the time domain and  $\tilde{a}_h[m] = a_h \exp(j2\pi f_{D, h} m T_0 + j\varphi_h)$  [8].

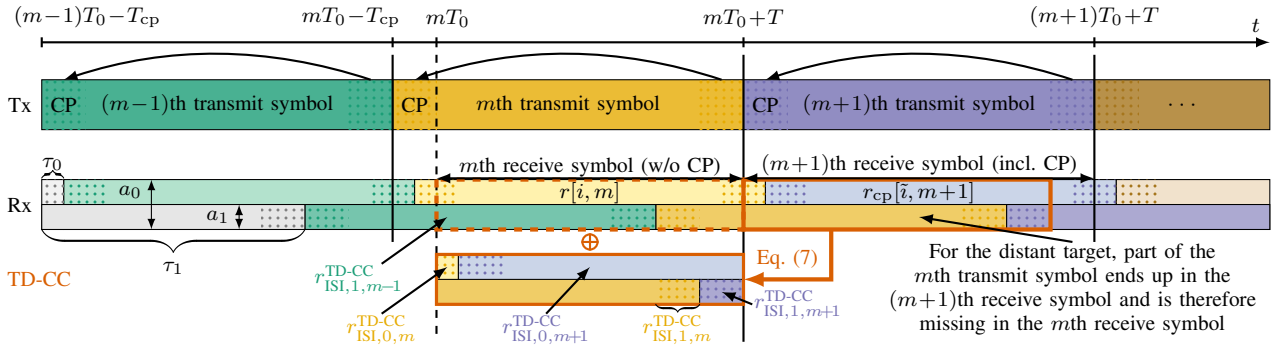


Fig. 3. The first and the second row visualize the transmit and receive signal in the case of a close and distant reflection, i.e., target, having an amplitude and delay of  $a_0, \tau_0$  and  $a_1, \tau_1$ , respectively. The third row and orange boxes visualize the proposed TD-CC: The  $N$  samples following the  $m$ th receive symbol are added to the  $m$ th receive symbol. The resulting ISI after TD-CC is labeled as in (9). We assume a synchronized transmitter and receiver in our monostatic setup. [1]

Figure 3 depicts the transmitted and received signals for two targets, one close and one distant, as well as the CC. It can be observed in the second row of Fig. 3 that, if a delay exceeds  $T_{cp}$ , part of the  $(m-1)$ th transmit symbol ends up in the  $m$ th receive symbol, leading to ISI. Additionally, the  $m$ th receive symbol does not contain the complete  $m$ th transmit OFDM symbol, leading to a reduced peak power and ICI [7]. In [7], analytical expressions for the peak power, ISI, ICI, and SINR for the received symbols  $Y$  in the FD are derived. We expand these results and give in the following the SINR in the RDM because it is a crucial metric for detection. For the sake of conciseness, we present only the key ideas of the derivation. The element-wise symbol division to estimate the channel does not change the power if QPSK is used. For the sake of simplicity, we assume that QPSK symbols are transmitted as they outperform higher order modulation formats for sensing due to noise enhancement [8]. The peak power experiences an integration gain  $G_P = MN$  due to the coherent addition in the (I)FFT. In contrast, the ISI and ICI are uncorrelated and retain the same power in the RDM as in the frequency domain due to Parseval's theorem. Our derived analytical expressions for the peak power, ISI, and ICI in the RDM are summarized in Tab. I.

### III. MULTI TARGET COHERENT COMPENSATION

In this section, we summarize and generalize the TD-CC proposed by [7], demonstrate its deficiency in a multi target scenario and propose our novel and robust MTCC.

#### A. Coherent Compensation

The TD-CC algorithm proposed in [7] is based on the observation that the  $m$ th receive OFDM symbol must contain the complete  $m$ th transmit OFDM symbol to have full peak power and to prevent ICI. Figure 3 shows that part of the  $m$ th transmit symbol ends up in the  $(m+1)$ th receive symbol if  $\tau_h > T_{cp}$ . Therefore, the TD-CC adds the samples of the  $(m+1)$ th received symbol belonging to the  $m$ th transmit symbol to the start of the  $m$ th receive symbol. However, this requires knowledge about the delay  $\tau_{TOI}$  of the TOI which should be detected, to determine the number of samples to be added, resulting in a chicken-and-egg problem. Further,

scenarios with multiple targets are not discussed in the original publication. Therefore, we generalize the TD-CC proposed in [7] to ensure that the complete  $m$ th transmit symbol is in the compensated  $m$ th receive symbol restoring the full peak power and preventing ICI for multiple targets with unknown delays  $0 \leq \tau_h < T$ . As depicted in Fig. 3, we propose to add the  $N$  samples following the  $m$ th receive symbol to the  $m$ th receive symbol, i.e., for  $\tilde{i}=1, \dots, N$

$$r_{cp}^{TD-CC}[\tilde{i} + N_{cp}, m] = r_{cp}[\tilde{i} + N_{cp}, m] + r_{cp}[\tilde{i}, m + 1]. \quad (7)$$

After TD-CC, the received reflection of the  $h$ th target without CP becomes a cyclically shifted version of the transmit signal

$$r_h^{TD-CC}[i, m] = \tilde{a}_h[m] \left( s[i + \frac{\tau_h}{T} \bmod N, m] + r_{ISI,h}^{TD-CC}[i, m] \right) \quad (8)$$

and an ISI term, which is

$$\begin{aligned} r_{ISI,h}^{TD-CC}[i, m] = & \underbrace{\sum_{n=1}^N X[n, m+1] e^{j2\pi n \Delta f (iT_s - \tau_h)} g(iT_s - \tau_h)}_{\tau_{ISI,h,m+1}^{TD-CC}} \\ & + \underbrace{\sum_{n=1}^N X[n, m] e^{j2\pi n \Delta f (iT_s + T_{cp} - \tau_h)} \text{rect}_{[-T_{cp}, 0)}(iT_s + T_{cp} - \tau_h)}_{\tau_{ISI,h,m}^{TD-CC}} \\ & + \underbrace{\sum_{n=1}^N X[n, m-1] e^{j2\pi n \Delta f (iT_s + T_0 - \tau_h)} g(iT_s - T - \tau_h)}_{\tau_{ISI,h,m-1}^{TD-CC}}. \end{aligned} \quad (9)$$

Equation (9) shows that additional ISI stemming from the  $m$ th and  $(m+1)$ th transmit symbol is introduced, where the ISI stems mainly from the  $(m+1)$ th transmit OFDM symbol for a close target. Additionally, the TD-CC doubles the thermal noise power and Tab. I summarizes the power levels.

The CC can be also carried out in the frequency domain by

$$Y^{FD-CC}[n, m] = Y[n, m] + C[n] \odot Y[n, m+1], \quad (10)$$

where  $C[n] = e^{-j2\pi n N_{cp}/N}$  compensates for the time delay introduced by the CP. Note that FD-CC performs slightly worse than TD-CC because the signal which arrives during the  $(m+1)$ th cyclic prefix is lost. This means that a residual ICI remains, as shown in Tab. I.

TABLE I

SUMMARY OF THE DERIVED PEAK, ISI AND ICI POWER OF THE  $h$ TH TARGET IN THE RDM ASSUMING A QPSK TRANSMISSION WHERE THE DERIVATION IS BASED ON [7]. FOR BREVITY, WE DEFINE  $T_{cp}^{\min} = \min(T_{cp}, (\tau_h - T_{cp})^+)$  AND  $(\cdot)^+ = \max(\cdot, 0)$ .

Name	No CC	TD-CC	FD-CC	MTCC
$P_{\text{Peak},h}$	$G_P a_h^2 \left(1 - \frac{(\tau_h - T_{cp})^+}{T}\right)^2$	$G_P a_h^2 \left(1 + \frac{\min(\tau_h, T_{cp})}{T}\right)$	$G_P a_h^2$	$G_P a_h^2$
$P_{\text{ISI},h}$	$a_h^2 \left(\frac{(\tau_h - T_{cp})^+}{T}\right)$	$a_h^2$	$a_h^2 \left(1 + \frac{T_{cp}^{\min}}{T}\right)$	$a_h^2 \frac{(\tau_h - T_{cp})^+}{T} + \min\left(a_h^2, \frac{\varepsilon}{G_P}\right) \frac{T - (\tau_h - T_{cp})^+}{T}$
$P_{\text{ICI},h}$	$a_h^2 \frac{(T - T_{cp} - \tau_h)(\tau_h - T_{cp})^+}{T^2}$	0	$a_h^2 \frac{(T - T_{cp}^{\min})T_{cp}^{\min}}{T^2}$	$2a_h^2 \frac{(T - T_{cp}^{\min})T_{cp}^{\min}}{T^2}$
$P_{\text{Therm}}$	$\sigma_{\text{Therm}}^2$	$2\sigma_{\text{Therm}}^2$	$2\sigma_{\text{Therm}}^2$	$2\sigma_{\text{Therm}}^2$

### B. Coherent Compensation in a Multi Target Scenario

To illustrate the drawback of the TD-CC in a multi target scenario, we consider a scenario with one close and one distant target, as depicted in Fig. 1. In conventional radar processing, only the distant target introduces ISI (see Sec. II-D). However, both targets introduce ISI when the TD-CC is applied. As illustrated in Fig. 3, the  $(m+1)$ th receive symbol contains not only the  $m$ th transmit symbol from the reflection of the distant target but also, predominantly, the  $(m+1)$ th transmit symbol from reflections of the close target. Since this consecutive receive symbol is added to the actual receive symbol to restore the peak power of the distant target, ISI from the  $(m+1)$ th transmit symbol is introduced into the  $m$ th symbol due to the close target (9). Given the reflected power decreases quartically with distance and the ISI power scales linearly with the reflected power  $a_h^2$  of the target, the ISI from the close target is dominant because it is usually much stronger than that of the distant target. Figure 4 shows a Doppler cut of the RDM after CC with various positions for the close target. We observe that this ISI manifests as a floor, which increases as the first target comes closer, preventing the detection of the distant target. This renders scenarios with both a close and distant target highly challenging. Therefore, we will consider these scenarios in the following. Further, Fig. 4 validates that the ISI is mainly caused by the close target in this multi target scenario.

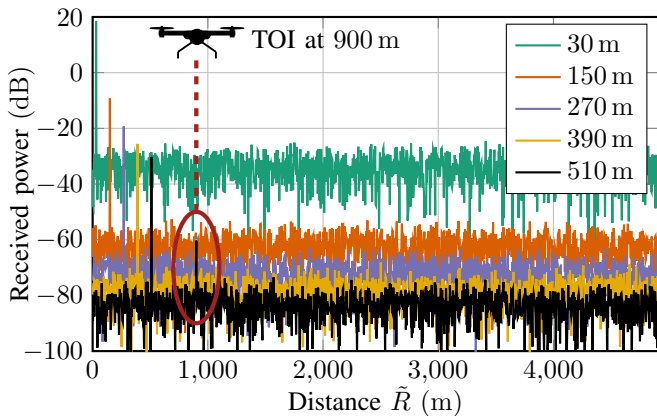


Fig. 4. RDM cut at  $\tilde{v} = 0$  after the TD-CC for a scenario with two static targets. The range of the first target is given by the legend, and the distance of the second target is fixed at  $R_2 = 900$  m. The RCS of the first and second target are  $\sigma_{\text{RCS},1} = 10 \text{ m}^2$  and  $\sigma_{\text{RCS},2} = 0.1 \text{ m}^2$  representing a truck and a drone, respectively. The ISI introduced by the first target becomes stronger as it gets closer, preventing the detection of the second target.

### C. Multi Target Coherent Compensation

TD-CC enhances the peak power of distant targets [7] but the overall performance deteriorates in multi target scenarios due to an increased interference-and-noise floor. To address this limitation, we propose a MTCC, a modified version of the FD-CC, which increases the peak power of the distant targets with only a minimal increase of the floor, ensuring a robust performance in multi target scenarios.

For the MTCC, we first compute the RDM without applying any CC, as detailed in Sec. II-C. Distant targets with small RCSs, which are of particular interest, may not be detected in this initial RDM using conventional radar processing. However, we note that in this initial RDM the close targets and the targets with a large RCS are detectable. We recall that these targets will generate strong ISI if the CC is applied.

Since the ISI after applying the CC scales linearly with the peak power  $a_h^2$  of the target (see Tab. I), we propose to limit the peak power of the targets in the RDM to a threshold  $\varepsilon \in \mathbb{R}^+$

$$\text{RDM}_T[\tilde{R}, \tilde{v}] = \begin{cases} \text{RDM}[\tilde{R}, \tilde{v}], & |\text{RDM}[\tilde{R}, \tilde{v}]|^2 < \varepsilon \\ \sqrt{\varepsilon}, & |\text{RDM}[\tilde{R}, \tilde{v}]|^2 \geq \varepsilon \end{cases} \quad (11)$$

to reduce the amount of ISI introduced by the CC. To avoid significant degradation of the image SINR, the ISI introduced by the CC should be below the thermal noise floor. Since the threshold  $\varepsilon$  limits the ISI to  $\varepsilon/G_P$  per target (see Tab. I) if the CC is applied,  $\varepsilon$  should be chosen such that  $\varepsilon < \sigma_{\text{Therm}}^2 G_P$ . However, it should be above the observed floor from the initial estimate, since it contains the signal components from the previous OFDM symbol.

Next, the RDM  $\text{RDM}_T$  with attenuated peaks is transformed back into the frequency domain, and the corresponding received signal with attenuated peaks is derived

$$Y_T[n, m] = \text{FFT}_{N \downarrow} \left\{ \text{IFFT}_{M \rightarrow} \left\{ \text{RDM}_T[\tilde{R}, \tilde{v}] \right\} \right\} \odot X[n, m]. \quad (12)$$

The derived received signal  $Y_T[n, m+1]$  is fed to the FD-CC defined in (10), where it replaces the received signal  $Y[n, m+1]$  and yields  $Y^{\text{MTCC}}$ . The final RDM  $\text{RDM}^{\text{MTCC}}$  is computed based on  $Y^{\text{MTCC}}$  as described in Sec. II-C.

The final RDM  $\text{RDM}^{\text{MTCC}}$  has attenuated peaks because it is based on  $\text{RDM}_T$  (11). Therefore,  $\text{RDM}^{\text{MTCC}}$  is combined with the initial RDM  $\text{RDM}$  to restore the height of the peaks. Our proposed MTCC adds only a slight increase in complexity, with the FFT efficiently implemented at a low level and otherwise requiring only pointwise operations, as summarized in Algorithm 1.



---

**Algorithm 1** Multi target coherent compensation (MTCC)

**Input:**  $X[n, m]$ ,  $Y[n, m]$ ,  $H_{\text{win}}[n, m]$ ,  $\varepsilon$ 

- 1:  $\text{RDM}[\tilde{R}, \tilde{v}] = \text{FFT}_{M \rightarrow} \left\{ \text{IFFT}_{N \downarrow} \left\{ \frac{Y[n, m]}{X[n, m]} \odot H_{\text{win}}[n, m] \right\} \right\}$
- 2:  $\text{RDM}_T[\tilde{R}, \tilde{v}] = \begin{cases} \text{RDM}[\tilde{R}, \tilde{v}], & |\text{RDM}[\tilde{R}, \tilde{v}]|^2 < \varepsilon \\ \sqrt{\varepsilon}, & |\text{RDM}[\tilde{R}, \tilde{v}]|^2 \geq \varepsilon \end{cases}$
- 3:  $Y_T[n, m] = \text{FFT}_{N \downarrow} \left\{ \text{IFFT}_{M \rightarrow} \left\{ \text{RDM}_T[\tilde{R}, \tilde{v}] \right\} \right\} \odot X[n, m]$
- 4:  $Y^{\text{MTCC}}[n, m] = Y[n, m] + C[n] \odot Y_T[n, m+1]$
- 5:  $\text{RDM}^{\text{MTCC}}[\tilde{R}, \tilde{v}] = \text{FFT}_{M \rightarrow} \left\{ \text{IFFT}_{N \downarrow} \left\{ \frac{Y^{\text{MTCC}}[n, m]}{X[n, m]} \right\} \right\}$
- 6:  $\text{RDM}^{\text{MTCC}}[\tilde{R}, \tilde{v}] = \begin{cases} \text{RDM}^{\text{MTCC}}[\tilde{R}, \tilde{v}], & |\text{RDM}[\tilde{R}, \tilde{v}]|^2 < \varepsilon \\ \text{RDM}[\tilde{R}, \tilde{v}], & |\text{RDM}[\tilde{R}, \tilde{v}]|^2 \geq \varepsilon \end{cases}$

**Return:**  $\text{RDM}^{\text{MTCC}}[\tilde{R}, \tilde{v}]$ 


---

#### D. Performance Metrics

We use the image SINR to assess the performance gain of our MTCC. We generalize the image signal-to-noise ratio [4] to include also the quantization noise, ISI and ICI stemming from targets exceeding the ISI-free range. The ISI and ICI manifest themselves as additive white Gaussian noise [10] and reduce the image SINR, which is defined for a TOI as

$$\text{Image SINR}_{\text{TOI}} = \frac{P_{\text{Peak, TOI}}}{P_{\text{Therm}} + P_Q + \sum_{h=1}^H (P_{\text{ISI}, h} + P_{\text{ICI}, h})}, \quad (13)$$

where the quantisation noise power is [11]

$$P_Q = \frac{P_{\text{Sig}} \cdot \text{PAPR}}{G_P \cdot 10 \log_{10} (6.02Q)}, \quad (14)$$

and  $P_{\text{Sig}}$  and PAPR denote the average signal power and peak-to-average power ratio of the received signal  $r(t)$ , respectively.

#### IV. SIMULATION RESULTS

In this section, we compare conventional radar processing (no-CC) [8], the generalized state-of-the-art TD-CC [7] and our proposed MTCC with a threshold of  $\varepsilon = 100P_{\text{Therm}}$ . Throughout the simulations, the modulation alphabet is QPSK, and the assumed TOI is a drone with a RCS of  $0.1 \text{ m}^2$ . For simplicity, we assume that the distance is a multiple integer of the range resolution and that the receiver applies a rectangular window  $H_{\text{win}}[n, m] = 1$ .

TABLE II  
CONSIDERED SYSTEM PARAMETRIZATIONS [11]

Parameter	Symbol	Full frame	Partial frame
Carrier frequency	$f_c$	3.5 GHz	3.5 GHz
Bandwidth	$B$	200 MHz	200 MHz
Sub-carrier spacing	$\Delta f$	30 kHz	30 kHz
No. sub-carrier	$N$	6552	6552
CP length (sample)	$N_{\text{cp}}$	458	458
No. OFDM symbols	$M$	280	10
Transmit power	$P_{\text{Tx}}$	49 dBm	49 dBm
Antenna gain	$G_{\text{Tx}}, G_{\text{Rx}}$	25.8 dBi	25.8 dBi
Noise figure	$F$	8 dB	8 dB

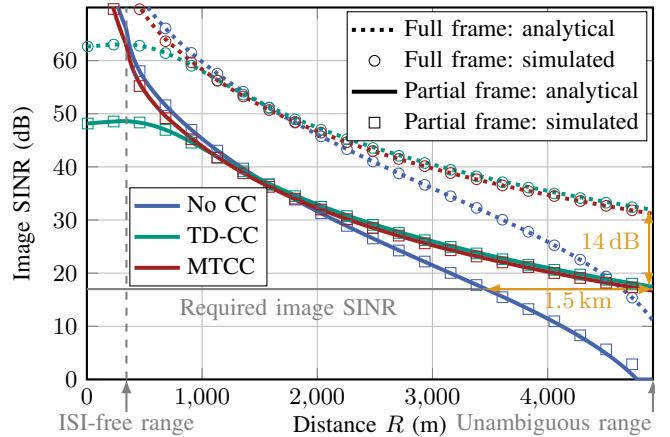


Fig. 5. Single target scenario: Image SINR as a function of its distance for the system parametrizations given in Tab. II with and without CC. For reliable detection, an image SINR of at least 17 dB is required [11].

#### A. Coherent Compensation in a Single Target Scenario

We first quantify the image SINR improvement of a CC in a scenario where only a single distant drone should be detected. Figure 5 shows the analytically derived and simulated image SINR as a function of the distance up to the unambiguous range  $R_{\text{max}} = Nc_0/(2B)$ , which is 4914 m for our parametrizations. Tab. II shows the two system parameterizations under investigation, a full frame and a partial frame using only 3.6% of the OFDM symbols for sensing [11]. For reliable performance in terms of both false alarms and missed detection, an image SINR of 17 dB is required [11]. We observe that a drone can generally be detected beyond the ISI-free range. However, the image SINR falls quickly below 17 dB, which would result in a missed detection for long distances without a CC mainly due to the reduced peak power (see Sec. II-D). On the contrary, our MTCC outperforms the classical OFDM radar processing after 1750 m, increases the drone detection distance up to the maximum range for both parametrizations, and improves the image SINR up to 14 dB at the unambiguous range. This means that the partial frame suffices for drone detection up to the unambiguous range and only 3.6% of the processing gains are required using the MTCC compared to no CC, resulting in 96.4% less overhead in terms of radio resources required.

#### B. Coherent Compensation in a Multi Target Scenario

Next, we add a second, interfering target close to the base station at  $R_{\text{Int}} = 105 \text{ m}$  with  $\sigma_{\text{RCS, Int}} = 10 \text{ m}^2$ , representing, e.g., a truck, to evaluate the performance of our algorithm in a multi target scenario. Figure 6 depicts the image SINR as a function of the range of the TOI, the drone. As in the single target scenario, distant targets cannot be detected using conventional OFDM radar processing. The image SINR after TD-CC degrades rapidly due to the ISI introduced by the second, interfering target (see Sec. III-B). On the contrary, our MTCC achieves the same SINR as in the single target scenario. This demonstrates that our proposed MTCC increases the peak power of the target without increasing the ISI power significantly enabling reliable long-range sensing in multi target scenarios.

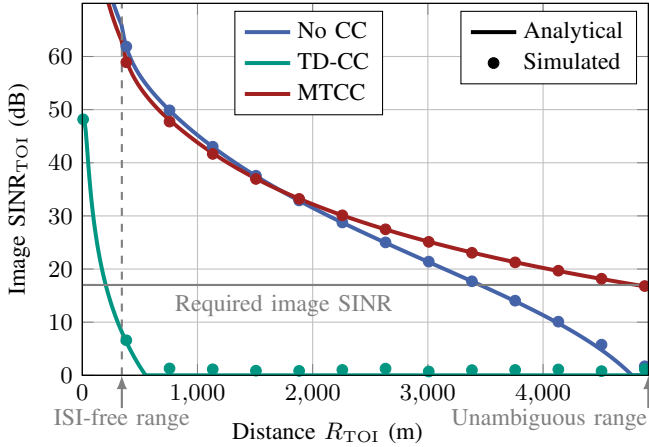


Fig. 6. Multi target scenario: Image SINR of the TOI as a function of its distance for the partial frame parametrization given in Tab. II with and without CC. The distance of the second, interfering target is fixed at  $R_{\text{Int}} = 105$  m.

### C. Scenario Analysis

Finally, we consider a scenario in which the TOI has a fixed distance  $R_{\text{TOI}} = 4500$  m. We sweep the distance and RCS of the interfering target to demonstrate the wide performance improvement of our proposed MTCC. Figure 7 shows the image SINR of the TOI as a function of the peak power of the interfering target  $P_{\text{Peak,Int}}$ .

Recall that TD-CC introduces ISI, which is  $G_P$  times weaker than the peak power. As indicated by the blue area in Fig. 7, if the peak power of the interfering target is small, the ISI introduced by CC is less than the thermal noise power, causing only minor performance degradation without the need for adaptation of the CC. Conversely, in the presence of an exceedingly strong interfering target, the quantization noise constrains the detection as indicated by the orange area in Fig. 7. Therefore, detecting the secondary target is not feasible even with our MTCC. However, note that our MTCC is more robust to quantization noise compared to no CC because the peak power of the TOI is larger (see Tab. I). If the peak power of the interferer lies between these two extremes, our method improves the image SINR by 13.2 dB compared to no CC, (due to reduced peak power) and enables reliable detection, where TD-CC fails (due to strong additional ISI). Therefore, Fig. 7 demonstrates the superior and robust performance of our proposed MTCC over variations up to 70 dB in the peak power of the interfering target, covering most realistic scenarios, where drones and buildings are interfering targets.

## V. CONCLUSION

CP-OFDM-ISAC systems suffer from a significant loss in image SINR when detecting distant objects because their corresponding path delays surpass the CP duration. We showed that existing algorithms are not suitable for multi target scenarios due to strong additional ISI. As a solution, we proposed MTCC, a novel and robust algorithm maintaining the image SINR in multi target scenarios. We derived analytical expressions for the image SINR and verified them through

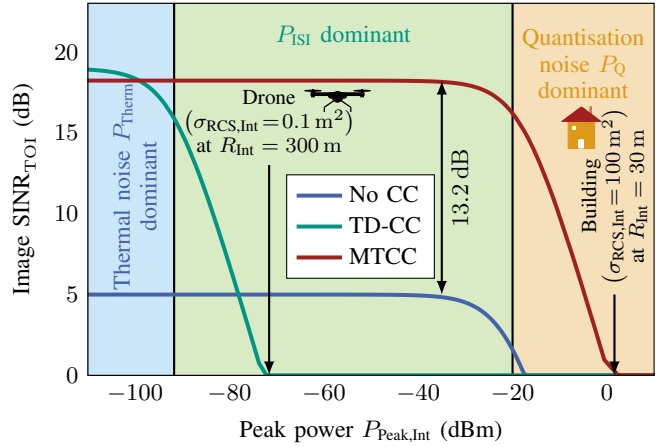


Fig. 7. Image SINR of the TOI (drone) as a function of the peak power of the interfering target. Specifically, a peak power  $P_{\text{Peak,Int}}$  of  $-71.6$  dBm and  $1.6$  dBm corresponds to a drone ( $\sigma_{\text{RCS,Int}} = 0.1 \text{ m}^2$ ) at a distance of  $R_{\text{Int}} = 300$  m and a building ( $\sigma_{\text{RCS,Int}} = 100 \text{ m}^2$ ) at a distance of  $R_{\text{Int}} = 30$  m, respectively.

numerical simulations. Our proposed MTCC increases the image SINR by up to 14 dB at long ranges. This allows less overhead of required radio resources to generate enough processing gain for reliable target detection, with up to 96.4% reductions in our numerical study. Our proposed MTCC paves the way for resource-efficient 6G ISAC systems that can master challenging tasks like long-range drone detection.

## REFERENCES

- [1] T. Wild, A. Grudnitsky, S. Mandelli, M. Henninger, J. Guan, and F. Schaich, "6G integrated sensing and communication: From vision to realization," in *Proc. European Radar Conference (EuRAD)*, 2023.
- [2] V. Shatov *et al.*, "Joint radar and communications: Architectures, use cases, aspects of radio access, signal processing, and hardware," *IEEE Access*, vol. 12, pp. 47 888–47 914, 2024.
- [3] 3GPP, "Feasibility study on integrated sensing and communication," Technical Specification Group TSG SA, Tech. Rep. 22.837 (Version 19.3.0), 2024.
- [4] B. Nuss, J. Mayer, and T. Zwick, "Limitations of MIMO and multi-user access for OFDM radar in automotive applications," in *Proc. IEEE International Conference on Microwaves for Intelligent Mobility (ICMIM)*, 2018.
- [5] 3GPP, "Physical channels and modulation," Technical Specification Group TSG SA, Tech. Rep. 38.211 (Version 18.2.0), 2024.
- [6] V. Oliari, A. Pandharipande, and W. Van Houtum, "OFDM radar sensing in joint communication and sensing systems without cyclic prefix overhead," *IEEE Sensors J.*, 2024.
- [7] L. Wang, Z. Wei, L. Su, Z. Feng, H. Wu, and D. Xue, "Coherent compensation based ISAC signal processing for long-range sensing," in *Proc. International Symposium on Modeling and Optimization in Mobile, Ad Hoc, and Wireless Networks (WiOpt)*, 2023, pp. 689–695.
- [8] M. Braun, "OFDM radar algorithms in mobile communication networks," Ph.D. dissertation, Karlsruhe Institute of Technology, 2014.
- [9] M. A. Richards, *Fundamentals of Radar Signal Processing*, 2nd ed. New York: McGraw-Hill Education, 2014.
- [10] J. Seoane, S. Wilson, and S. Gelfand, "Analysis of intertone and interblock interference in OFDM when the length of the cyclic prefix is shorter than the length of the impulse response of the channel," in *Proc. IEEE Global Telecommunications Conference (GLOBECOM)*, 1997, pp. 32–36.
- [11] S. Mandelli, M. Henninger, M. Bauhofer, and T. Wild, "Survey on integrated sensing and communication performance modeling and use cases feasibility," in *Proc. International Conference on 6G Networking (6GNet)*, 2023.